




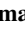
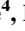







## Emission Characteristics of Greenhouse Gases and Air Pollutants in Northern Hemisphere Cities: Comprehensive Assessment Using Ground-Based Fourier Transform Spectrometers

### Key Points:

- We comprehensively assessed the emission characteristics of greenhouse gases and air pollutants in seven cities in the Northern Hemisphere
- Ground-based Fourier transform spectrometers offers a comprehensive analysis of the urban emission characteristics of greenhouse gases and air pollutants
- Our results can further support effective strategies for mitigating climate change

Jonghyuk Lee<sup>1,2</sup> , Sujong Jeong<sup>1,2</sup> , Hayoung Park<sup>1</sup> , Jaemin Hong<sup>1,2</sup> , Jueun Kim<sup>1</sup>, Matthias Max Frey<sup>3</sup> , Isamu Morino<sup>3</sup> , Hirofumi Ohyama<sup>3</sup> , Frank Hase<sup>4</sup>, Marios Mermigkas<sup>5</sup> , Minqiang Zhou<sup>6</sup> , Yao Té<sup>7</sup> , and Coleen M. Roehl<sup>8</sup>

<sup>1</sup>Department of Environmental Planning, Graduate School of Environmental Studies, Seoul National University, Seoul, Republic of Korea, <sup>2</sup>Climate Tech Center, Seoul National University, Seoul, Republic of Korea, <sup>3</sup>Earth System Division, National Institute for Environmental Studies, Tsukuba, Japan, <sup>4</sup>Institute of Meteorology and Climate Research (IMK-ASF), Karlsruhe Institute of Technology (KIT), Karlsruhe, Germany, <sup>5</sup>Laboratory of Atmospheric Physics, Department of Physics, Aristotle University of Thessaloniki, Thessaloniki, Greece, <sup>6</sup>Institute of Atmospheric Physics, Chinese Academy of Sciences, Beijing, China, <sup>7</sup>Laboratoire d'Études du Rayonnement et de la Matière en Astrophysique et Atmosphères (LERMA-IPSL), Observatoire de Paris, CNRS, Sorbonne Université, PSL Université, Paris, France, <sup>8</sup>Division of Geological and Planetary Sciences, California Institute of Technology, Pasadena, CA, USA

### Correspondence to:

S. Jeong,  
[sujung@snu.ac.kr](mailto:sujung@snu.ac.kr)

### Citation:

Lee, J., Jeong, S., Park, H., Hong, J., Kim, J., Frey, M. M., et al. (2024). Emission characteristics of greenhouse gases and air pollutants in Northern Hemisphere cities: Comprehensive assessment using ground-based Fourier transform spectrometers. *Journal of Geophysical Research: Atmospheres*, 129, e2023JD040562. <https://doi.org/10.1029/2023JD040562>

Received 18 JAN 2024  
Accepted 5 JUN 2024

**Abstract** Despite the importance of understanding the urban emission characteristics of greenhouse gases (GHGs) and air pollutants, few studies have conducted integrated assessments across diverse urban environments. Herein, we conducted a comprehensive evaluation of the emission characteristics of GHGs and air pollutants in seven cities in the Northern Hemisphere using ground-based Fourier transform spectrometers. Our analysis primarily focused on emission ratios of excess column-averaged dry-air mole fractions of carbon monoxide (CO) to carbon dioxide (CO<sub>2</sub>) ( $\Delta X_{CO}:\Delta X_{CO_2}$ ) and those of methane (CH<sub>4</sub>) to CO<sub>2</sub> ( $\Delta X_{CH_4}:\Delta X_{CO_2}$ ). We found that the emission ratios varied significantly across cities. Xianghe (China) and Pasadena (USA), known for severe air pollution, showed the highest emission ratios. Notably, Seoul (South Korea) showed lower  $\Delta X_{CO}:\Delta X_{CO_2}$  ( $3.32 \pm 0.10$  ppb/ppm) but relatively higher  $\Delta X_{CH_4}:\Delta X_{CO_2}$  ( $4.85 \pm 0.04$  ppb/ppm), which was comparable to the  $\Delta X_{CH_4}:\Delta X_{CO_2}$  value of Xianghe ( $5.15 \pm 0.10$  ppb/ppm), suggesting that targeted CH<sub>4</sub> reduction strategies may be required for climate change mitigation in Seoul.

**Plain Language Summary** Many cities experience significant greenhouse gas and air pollutant emissions. We comprehensively analyzed the characteristics of these emissions using ground-based solar-viewing Fourier transform spectrometers (FTSs) in Northern Hemisphere cities including Seoul (South Korea), Thessaloniki (Greece), Tsukuba (Japan), Karlsruhe (Germany), Xianghe (China), Pasadena (USA), and Paris (France). First, we focused on variations in carbon dioxide (CO<sub>2</sub>), methane (CH<sub>4</sub>), and carbon monoxide (CO). Based on these variations, their emission ratios were estimated in terms of excess column-averaged dry-air mole fractions of CO to CO<sub>2</sub> ( $\Delta X_{CO}:\Delta X_{CO_2}$ ) and CH<sub>4</sub> to CO<sub>2</sub> ( $\Delta X_{CH_4}:\Delta X_{CO_2}$ ) in urban sites. We found that the emission ratios differed across cities. For example, Xianghe and Pasadena, which generally exhibit high levels of air pollution, had the highest emission ratios. However, Seoul had lower emission ratios of  $\Delta X_{CO}:\Delta X_{CO_2}$ , but higher levels of  $\Delta X_{CH_4}:\Delta X_{CO_2}$ . This study suggests that ground-based Fourier transform spectrometer measurements can be used as a tool for comprehensively evaluating the emission characteristics of greenhouse gases and air pollutants in urban environments. Furthermore, extending our study to longer periods and more sites could further aid in formulating effective mitigation strategies for climate change.

## 1. Introduction

Carbon dioxide (CO<sub>2</sub>) and methane (CH<sub>4</sub>) are two primary greenhouse gases (GHGs) that contribute significantly to climate change. Carbon monoxide (CO) is an air pollutant and a precursor gas for ozone formation; it also has indirect effects on global warming (IPCC, 2007). Most anthropogenic emissions of GHGs and air pollutants originate from urban areas, leading to increasing concerns about their impacts on climate, environment, and air quality (Crippa et al., 2021). To address these issues effectively, a comprehensive understanding of the emission sources and characteristics of GHGs and air pollutants in urban regions is essential. This understanding serves as a

© 2024. The Author(s).

This is an open access article under the terms of the [Creative Commons Attribution License](https://creativecommons.org/licenses/by/4.0/), which permits use, distribution and reproduction in any medium, provided the original work is properly cited.

basis for developing effective strategies and policies to mitigate emissions from urban environments. Multiple studies have analyzed anthropogenic urban emissions (Silva et al., 2013; Wennberg et al., 2012; Wong et al., 2015). However, integrated assessments of atmospheric GHG and pollutant emissions in urban regions remain limited.

The emission ratio, which indicates the relationship between the emissions of a particular species and that of a reference species (Andreae & Merlet, 2001), is frequently used as a metric to estimate emission characteristics. Numerous studies have used satellite measurements to evaluate the emission characteristics of GHGs and air pollutants in urban areas. For instance, Silva et al. (2013) analyzed the CO<sub>2</sub>/CO emission ratio over megacities using the Greenhouse gases Observing SATellite (GOSAT; Kuze et al., 2009) and Measurements of Pollution in the Troposphere (MOPITT; Deeter et al., 2003). Recently, Park, Jeong, Park, et al. (2021) employed the Orbiting Carbon Observatory-2 (OCO-2; Eldering et al., 2017) and Sentinel-5 Precursor TROPOspheric Monitoring Instrument (S-5P TROPOMI; Veeffkind et al., 2012) to assess the emission characteristics of cities in the Northern Hemisphere based on both CO/CO<sub>2</sub> and NO<sub>2</sub>/CO<sub>2</sub> emission ratios. Although this satellite-based approach offers the capability to conduct multiregional analysis based on its global coverage and high accuracy, continuous analysis can be challenging owing to the poor temporal resolution of satellite data. For instance, OCO-2 has a repeat cycle of 16 days, and GOSAT and GOSAT-2 have repeat cycles of 3 and 6 days, respectively. Due to these relatively long repeat cycles, there is a lack of satellite data for urban areas. In contrast, ground-based measurements offer more detailed temporal variations and have thus been used to estimate the emission characteristics of the aforementioned GHGs and air pollutants in urban areas. Wunch et al. (2009) used ground-based IFS125HR Fourier transform spectrometer (FTS) measurements to estimate GHG emissions in California, USA. In addition, Wong et al. (2015) employed ground-based California Laboratory for Atmospheric Remote Sensing (CLARS)-FTS data to analyze CH<sub>4</sub>/CO<sub>2</sub> emission ratios in the megacity of Los Angeles (USA). However, these studies have focused on smaller areas or specific cities, and there is still a lack of comprehensive analyses regarding the emission characteristics of GHGs and air pollutants across multiple cities.

The present study aimed to be the first to comprehensively evaluate the emission characteristics of GHGs and air pollutants in cities in the Northern Hemisphere using ground-based FTS measurements. We used ground-based column data from two prominent global observation networks, the Total Carbon Column Observing Network (TCCON) (Wunch et al., 2011) and the COllaborative Carbon Column Observing Network (COCCON) (Frey et al., 2019). These networks can retrieve reliable long-term column-averaged dry-air mole fractions of GHGs and other atmospheric constituents, referred to as X<sub>gas</sub> (e.g., XCO<sub>2</sub>), using the IFS125HR (TCCON) and EM27/SUN (COCCON) spectrometers, respectively. We focused on cities in the Northern Hemisphere because urban environments predominantly located in this region, and the majority of TCCON and COCCON ground stations in urban areas are also located in the Northern Hemisphere. Our study focused on seven cities (Seoul, Thessaloniki, Tsukuba, Karlsruhe, Xianghe, Pasadena, and Paris) in 2021 where data sets for all cities were available. The remainder of this paper is organized as follows: Section 2 provides a concise overview of the TCCON and COCCON measurements. Section 3 presents the estimated emission characteristics for mid-latitude cities in the Northern Hemisphere, focusing on the variations in XCO<sub>2</sub>, XCH<sub>4</sub>, and XCO and their emission ratios (CO/CO<sub>2</sub> and CH<sub>4</sub>/CO<sub>2</sub>). Finally, Section 4 provides a comprehensive discussion and conclusions based on our findings, and summarizes the key insights and implications of this study.

## 2. Data and Methods

### 2.1. EM27/SUN

The portable EM27/SUN spectrometer (Gisi et al., 2012; Hase et al., 2016), developed collaboratively by the Karlsruhe Institute of Technology (KIT) and Bruker (Germany), can record solar absorption spectra in the near-infrared spectral range (4,000–11,000 cm<sup>-1</sup>) at a spectral resolution of 0.5 cm<sup>-1</sup>. This spectrometer retrieves the XCO<sub>2</sub>, XCH<sub>4</sub>, and XCO data from the measured spectra using the PROFFAST nonlinear least squares fitting algorithm developed by KIT and funded the European Space Agency (ESA) in the framework of the COCCON-PROCEEDS project (Alberti et al., 2022). The detailed X<sub>gas</sub> retrieval process has been described in several studies (e.g., Sha et al., 2020). This portable instrument has the advantage of simultaneously measuring a wide range of gases and are well-suited for use in urban environments. The unprecedented performance and stability of the EM27/SUN spectrometer has been validated in previous studies (Alberti et al., 2022; Frey et al., 2015, 2019; Sha et al., 2020). Furthermore, the portability of this spectrometer has facilitated its successful use in various field

campaigns (Butz et al., 2017, 2022; Klappenbach et al., 2015; Knapp et al., 2021; Luther et al., 2019; Makarova et al., 2021; Pak et al., 2023; Viatte et al., 2017).

## 2.2. IFS125HR

The IFS125HR spectrometer, which is the primary instrument in the TCCON network, operates at a spectral resolution of  $0.02 \text{ cm}^{-1}$ . This spectrometer retrieves the Xgas data from the near-infrared measured spectra using the GFIT nonlinear least squares fitting algorithm, which is the core component of the GGG processing software (Wunch et al., 2015). Recently, the TCCON Xgas data sets, processed using the newest GGG2020 software, were publicly released in April 2022. This study used the GGG2020 data products, as detailed in Laughner et al. (2023). Xgas retrieval in the IFS125HR has been thoroughly documented in several studies (Wunch et al., 2009, 2015) and is similar to the process used by the EM27/SUN spectrometer. These high-resolution instruments facilitate precise and accurate measurements of atmospheric gases, contributing to a comprehensive understanding of their distribution and behavior in the atmosphere. Furthermore, they play a crucial role in the validation of satellite measurements such as those from the OCO and GOSAT series.

## 2.3. OCO-2

OCO-2 (Crisp et al., 2017; Eldering et al., 2017), launched on 2 July 2014, is the first National Aeronautics and Space Administration (NASA) satellite dedicated to measuring global XCO<sub>2</sub> with high precision and accuracy. Its grating spectrometers collect high-resolution spectra of sunlight reflected from the Earth's surface across three spectral bands: the O<sub>2</sub>-A band at 0.765  $\mu\text{m}$ , the weak CO<sub>2</sub> band at 1.61  $\mu\text{m}$ , and the strong CO<sub>2</sub> band at 2.06  $\mu\text{m}$ . Coincident measurements from these bands are analyzed using the optimal estimation-based algorithm (O'Dell et al., 2012) to retrieve XCO<sub>2</sub>. OCO-2 operates in a sun-synchronous orbit at an altitude of 705 km, with an Equatorial Crossing Time (ECT) of approximately 13:36 for ascending node. Its swath width is approximately 10 km, offering a 16-day repeat cycle with spatial resolutions of 1.29 km (cross-track)  $\times$  2.25 km (along-track). In this study, we used the OCO-2 Level 2 Lite version 11 product. To ensure data reliability, OCO-2 XCO<sub>2</sub> data sets were filtered using the "xco2\_quality\_flag" parameter provided in the data product, specifically selecting only those XCO<sub>2</sub> measurements with xco2\_quality\_flag of 0. This filtering is recommended by the OCO-2 Data Product User's Guide ([https://disc.gsfc.nasa.gov/datasets/OCO2\\_L2\\_Lite\\_FP\\_11.1r/summary?keywords=OCO-2](https://disc.gsfc.nasa.gov/datasets/OCO2_L2_Lite_FP_11.1r/summary?keywords=OCO-2), last accessed: 31 March 2024).

## 2.4. S-5P TROPOMI

The S-5P, successfully launched on 13 October 2017, is the first satellite of the European Union's Copernicus program dedicated to the comprehensive monitoring of Earth's atmosphere. It is equipped with the TROPOMI (Veefkind et al., 2012), a push-broom spectrometer designed to measure the spectral data across the ultraviolet-visible (270–500 nm), the near-infrared (675–775 nm), and the shortwave infrared (2,305–2,385 nm) bands. These spectral measurements are used to retrieve column abundances of atmospheric trace gases, including CH<sub>4</sub>, CO, ozone (O<sub>3</sub>), nitrogen dioxide (NO<sub>2</sub>), and sulfur dioxide (SO<sub>2</sub>), as well as aerosol properties. The S-5P operates in a sun-synchronous orbit at an altitude of 824 km, with an ECT of approximately 13:30 for ascending node. TROPOMI has a wide swath width of approximately 2,600 km, enabling near-daily global coverage. In this study, the offline (OFFL) TROPOMI Level 2 data products for CH<sub>4</sub> and CO were used, applying quality filters based on the "qa\_value" parameter provided in the data products. Specifically, we selected only those data for both TROPOMI CH<sub>4</sub> and CO where qa\_value was greater than 0.5, as recommended by the S-5P product readme files (<https://sentinel.esa.int/documents/247904/3541451/Sentinel-5P-Methane-Product-Readme-File> for TROPOMI CH<sub>4</sub>; <https://sentinel.esa.int/documents/247904/3541451/Sentinel-5P-Carbon-Monoxide-Level-2-Product-Readme-File> for TROPOMI CO, last accessed: 31 March 2024). On 6 August 2019, the spatial resolution for TROPOMI CH<sub>4</sub> and CO products was improved from 7.0 km (cross-track)  $\times$  7.0 km (along-track) to 5.5 km (cross-track)  $\times$  7.0 km (along-track), enhancing its capability for detailed atmospheric measurements.

## 2.5. Estimation of Emission Ratios

In urban environments, the emission ratio of CO to CO<sub>2</sub> can provide insights into the types of fossil fuels used and their combustion efficiency (Chandra et al., 2016; Che et al., 2022; Sim et al., 2020). Additionally, the emission

**Table 1**  
*List of Ground-Based Fourier Transform Spectrometer Stations Used in This Study*

Station	Latitude	Longitude	Height (m)	FTS instrument
Seoul (South Korea)	37.464°N	126.954°E	98	EM27/SUN (COCCON)
Thessaloniki (Greece)	40.634°N	22.956°E	67	EM27/SUN (COCCON)
Tsukuba (Japan)	36.051°N	140.121°E	40	EM27/SUN (COCCON)
Karlsruhe (Germany)	49.012°N	8.444°E	133	EM27/SUN (COCCON)
Xianghe (China)	39.800°N	116.960°E	40	IFS125HR (TCCON)
Pasadena (USA)	34.140°N	−118.130°E	40	IFS125HR (TCCON)
Paris (France)	48.850°N	2.360°E	60	IFS125HR (TCCON)

ratio of CH<sub>4</sub> to CO<sub>2</sub> has been demonstrated as a simple and practical parameter for estimating urban CH<sub>4</sub> emissions (Hedelius et al., 2018; Wennberg et al., 2012; Wong et al., 2015; Wunch et al., 2009).

To estimate the emission ratios of anthropogenic gases, considering the background concentration, which refers to the concentration levels that remain unaffected by urban emissions, is essential when examining the observed gas concentration values. Relying solely on observed concentrations can hinder the interpretation of emission contributions. A method used in previous studies (Bares et al., 2018; Chandra et al., 2016; Park, Jeong, Koo, et al., 2021, 2022; Sim et al., 2020; Worthy et al., 2009) was employed in this study to determine the background concentration of the studied gas. This method involves determining the lower percentile (e.g., the lowest first or fifth percentile) of the measurements (XCO<sub>2</sub>, XCH<sub>4</sub>, and XCO) throughout the day as the daily background concentrations. Herein, we defined the daily background concentrations of XCO<sub>2</sub>, XCH<sub>4</sub>, and XCO as the lowest fifth percentile of these measurements. Subsequently, we calculated the excess XCO<sub>2</sub> (ΔXCO<sub>2</sub>), XCH<sub>4</sub> (ΔXCH<sub>4</sub>), and XCO (ΔXCO) by subtracting the daily background concentrations from the daily observed values using Equation 1:

$$\Delta X_{\text{gas}} = X_{\text{gas}} - X_{\text{gas}_b} \quad (1)$$

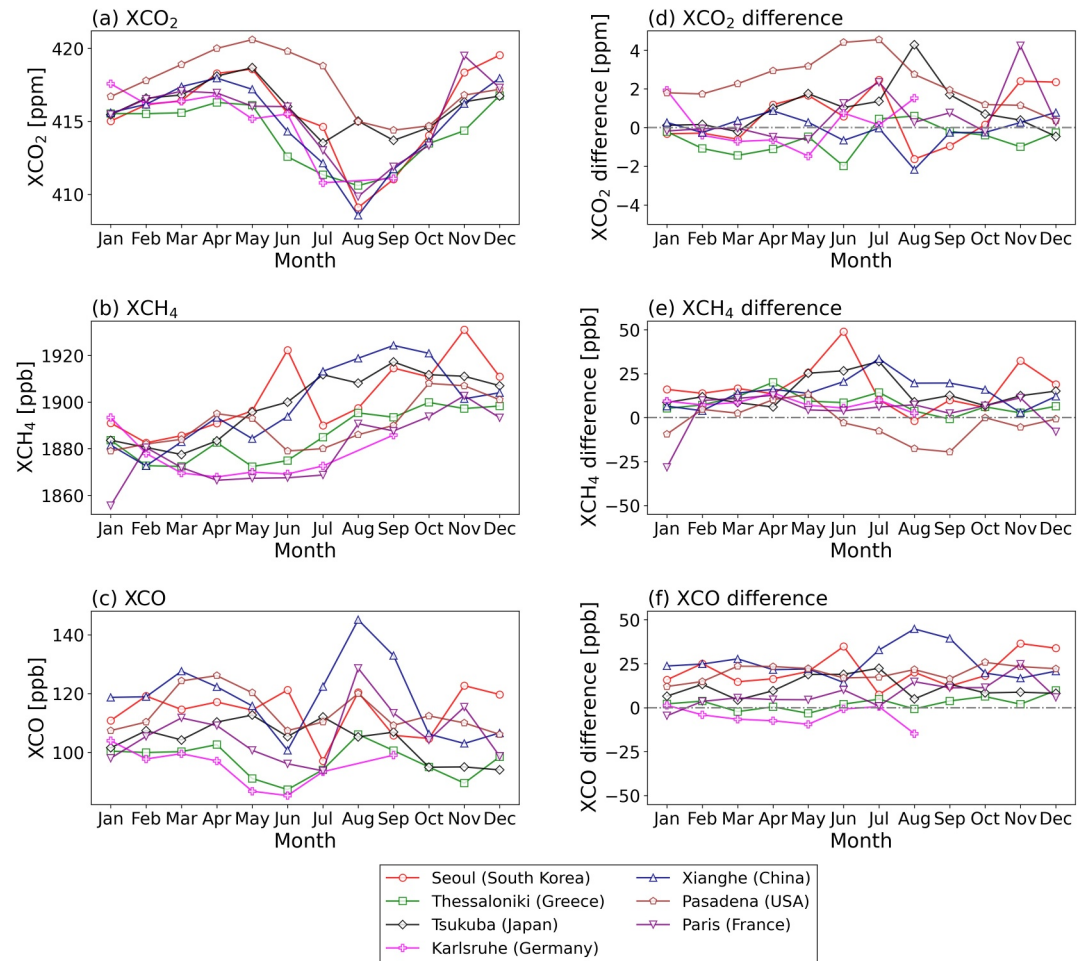
where ΔX<sub>gas</sub> represents the excess column-averaged dry-air mole fractions of the studied gas compared to the background levels and X<sub>gas<sub>b</sub></sub> refers to the daily background column-averaged dry-air mole fractions of the studied gas.

After calculating ΔXCO<sub>2</sub>, ΔXCH<sub>4</sub>, and ΔXCO, we performed a linear regression analysis to estimate the emission ratios of ΔXCO:ΔXCO<sub>2</sub> and ΔXCH<sub>4</sub>:ΔXCO<sub>2</sub>, represented by the slopes of the regression lines between the two species.

### 3. Results

#### 3.1. Monthly Median Timeseries of XCO<sub>2</sub>, XCH<sub>4</sub>, and XCO

Our analysis was based on continuous atmospheric measurements of XCO<sub>2</sub>, XCH<sub>4</sub>, and XCO obtained from ground-based FTS instruments. The ground-based FTS stations used in this study are listed in Table 1. These stations are located in Seoul, South Korea; Thessaloniki, Greece (<https://doi.org/10.48477/coccon.pf10.thessaloniki.R01> accessed on 04 September 2023); Tsukuba, Japan (<https://doi.org/10.48477/coccon.pf10.tsukuba.R02> accessed on 04 September 2023); Karlsruhe, Germany (<https://doi.org/10.48477/coccon.pf10.karlsruhe.R02> accessed on 04 September 2023); Xianghe, China (Zhou et al., 2022); Pasadena, USA (Wennberg et al., 2022); and Paris, France (Té et al., 2022). Our analysis focused on data from 2021 because this was the only year that data were consistently available across all seven ground-based FTS stations. While TCCON data can be accessed over a more extended period, the availability of COCCON data is limited to recent years, influencing our choice of the study period. The urban sites in Karlsruhe and Tsukuba provide TCCON data, in addition to COCCON data. However, the TCCON data for Tsukuba, available from the TCCON Data Archive (<https://tccodata.org>), covers the period from 28 March 2014 to 31 March 2021, which lacks complete data for our focus year of 2021. Likewise, the TCCON data for Karlsruhe, which covers the period from 15 January 2014 to 20 January 2023,



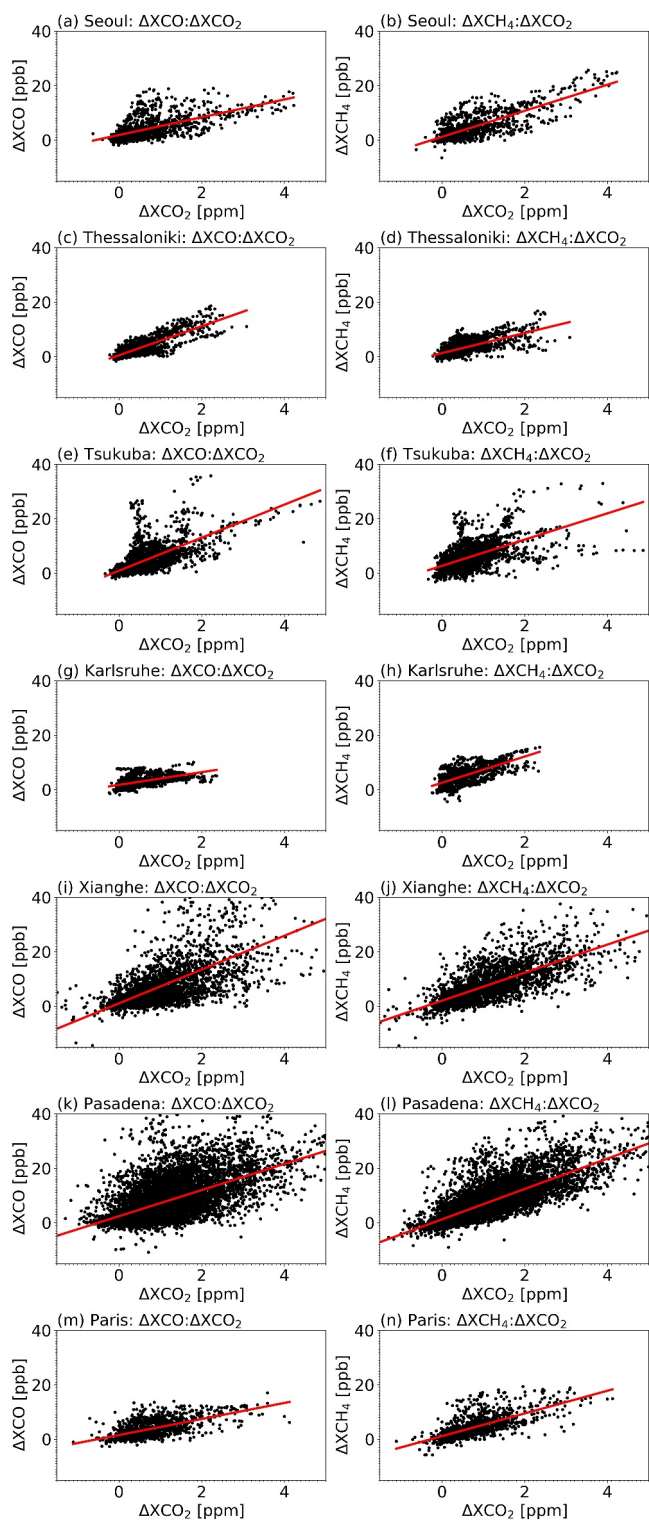
**Figure 1.** Monthly median variations in (a) XCO<sub>2</sub>, (b) XCH<sub>4</sub>, and (c) XCO at seven urban sites in the mid-latitude Northern Hemisphere (Seoul, Thessaloniki, Tsukuba, Karlsruhe, Xianghe, Pasadena, and Paris) throughout 2021, along with differences between the monthly median ground-based (d) XCO<sub>2</sub>, (e) XCH<sub>4</sub>, and (f) XCO values and their zonal median observations from the satellites (XCO<sub>2</sub> from OCO-2 and XCH<sub>4</sub> and XCO from S-5P TROPOMI).

includes data only from August to December in 2021. Due to these limitations in data coverage for the year of our study, we did not include the TCCON data from Karlsruhe and Tsukuba in our comparison analysis.

Figures 1a–1c present the monthly median variations in XCO<sub>2</sub>, XCH<sub>4</sub>, and XCO, respectively, in urban environments across the mid-latitude Northern Hemisphere throughout 2021. As expected, the XCO<sub>2</sub> values showed a clear seasonal cycle, with lower levels during summer (June–August) and higher levels during winter (December–February) and spring (March–May), as depicted in Figure 1a. Pasadena generally presented the highest XCO<sub>2</sub> levels, whereas the other cities showed comparatively lower levels, and the differences among cities were not substantial. In the case of the XCH<sub>4</sub> levels (Figure 1b), Seoul, Xianghe, and Tsukuba had higher values throughout the year, with Xianghe exhibiting the highest XCH<sub>4</sub> levels (approximately 1,920 ppb) from July to October. In contrast, Paris and Karlsruhe consistently exhibited lower XCH<sub>4</sub> levels. Furthermore, Seoul, Xianghe, and Pasadena had higher XCO levels compared to the other cities (Figure 1c). Xianghe generally exhibited the highest levels, with a monthly median XCO value of 145.1 ppb in August. In contrast, Thessaloniki and Karlsruhe consistently showed lower XCO levels, typically less than approximately 100 ppb.

Considering that the observed ground-based values shown in Figures 1a–1c might be reflected in regional trends, we further compared the measurements of XCO<sub>2</sub>, XCH<sub>4</sub>, and XCO with their corresponding satellite zonal median values. The zonal median values represent the median of satellite measurements over a certain range of latitudes. Figures 1d–1f show the differences between the monthly median ground-based XCO<sub>2</sub>, XCH<sub>4</sub>, and XCO





**Figure 2.** Scatterplots of  $\Delta XCO$  versus  $\Delta XCO_2$  (left columns) and  $\Delta XCH_4$  versus  $\Delta XCO_2$  (right columns) in seven urban sites for 2021. The red solid line in each sub-plot represents the regression line fitted to the data points.

values and their zonal median observations from the satellites ( $XCO_2$  from OCO-2 and  $XCH_4$  and  $XCO$  from S-5P TROPOMI). TROPOMI official Level 2 CO product was used as the total column density data ( $\text{mol}/\text{m}^2$ ). For comparison with ground-based XCO measurements, we converted the TROPOMI CO total column density to XCO (ppb) by dividing the total column density of CO by that of dry air (Sha et al., 2021; Wunch et al., 2011). For both the OCO-2 and S-5P TROPOMI measurements, the zonal median was calculated at  $5^\circ$ -latitude intervals to ensure a large sample size of satellite measurements. The trends observed in the zonal median differences, as illustrated in Figures 1d–1f, were in alignment with the specific gas concentration characteristics of each urban site depicted in Figures 1a–1c. This result suggests that ground-based measurements are effectively capture localized atmospheric conditions relevant to GHGs and air pollutants. Based on this finding, we aim to further estimate the emission characteristics of GHGs and air pollutants in urban areas using ground-based FTS measurements. The detailed analysis of the emission characteristics for each urban site is thoroughly discussed in Section 3.2.

### 3.2. Emission Ratios of $\Delta XCO:\Delta XCO_2$ and $\Delta XCH_4:\Delta XCO_2$

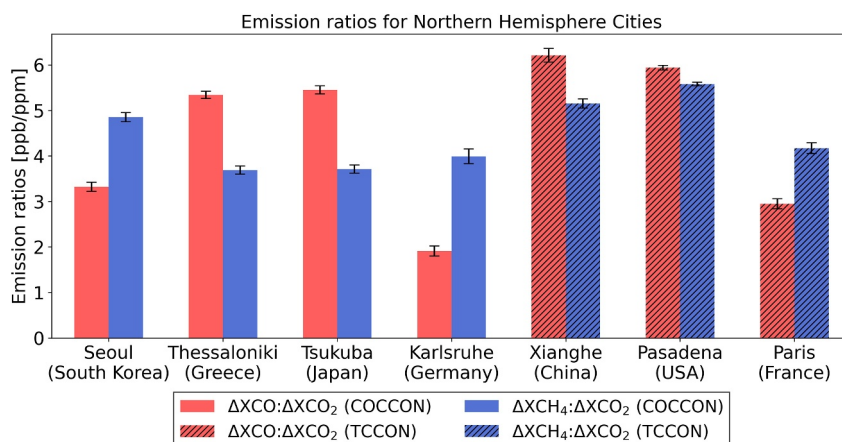
Based on the continuous atmospheric column measurements of  $XCO_2$ ,  $XCH_4$ , and  $XCO$  (Section 3.1), we investigated the emission ratios of  $\Delta XCO:\Delta XCO_2$  and  $\Delta XCH_4:\Delta XCO_2$  in seven urban sites. The linear regression method described in Section 2.5 was used to estimate the emission ratios.

Figure 2 shows the scatterplots of  $\Delta XCO$  versus  $\Delta XCO_2$  (left columns) and  $\Delta XCH_4$  versus  $\Delta XCO_2$  (right columns) in urban sites for 2021. The solid red line in each sub-plot represents the regression line fitted to the data points. As shown in Figure 2, the  $\Delta XCO$  versus  $\Delta XCO_2$  and  $\Delta XCH_4$  versus  $\Delta XCO_2$  plots exhibited distinct linear trends in all the cities (correlation coefficient  $>0.5$ ).

To comprehensively evaluate the emission characteristics of the seven cities located in the mid-latitude region of the Northern Hemisphere, we compared the emission ratios obtained by calculating the slopes of the regression lines, as shown in Figure 2. Figure 3 presents the emission ratios of  $\Delta XCO:\Delta XCO_2$  and  $\Delta XCH_4:\Delta XCO_2$  for each city, represented by red and blue bars, respectively. The emission ratio of  $\Delta XCO:\Delta XCO_2$  in Xianghe was  $6.21 \pm 0.15$  ppb/ppm, representing the highest emission ratio among the cities. Pasadena and Thessaloniki followed closely with estimated emission ratios of  $5.94 \pm 0.05$  ppb/ppm and  $5.34 \pm 0.18$  ppb/ppm, respectively. Conversely, Seoul, Paris, and Karlsruhe displayed comparatively lower  $\Delta XCO:\Delta XCO_2$  emission ratios. In terms of the emission ratio of  $\Delta XCH_4:\Delta XCO_2$ , Pasadena was the leading city ( $5.58 \pm 0.04$  ppb/ppm), followed by Xianghe ( $5.15 \pm 0.10$  ppb/ppm). Notably, Seoul showed a relatively high emission ratio of  $\Delta XCH_4:\Delta XCO_2$  ( $4.85 \pm 0.10$  ppb/ppm), which was comparable to that of Xianghe. Furthermore, Thessaloniki and Tsukuba displayed the lowest  $\Delta XCH_4:\Delta XCO_2$  emission ratios of  $3.69 \pm 0.09$  and  $3.71 \pm 0.09$  ppb/ppm, respectively.

In Figure 3, the urban sites in Xianghe and Pasadena exhibited broader distributions between the two species (Figures 3i–3l), compared to other urban sites. We further analyzed the seasonal distribution for these sites, which is

represented in Figures 4 and 5 for Xianghe and Pasadena, respectively. Note that the  $x$  and  $y$  axes ranges have been adjusted to enhance clarity, compared to those in Figure 3. Overall, the broader distributions in Xianghe and



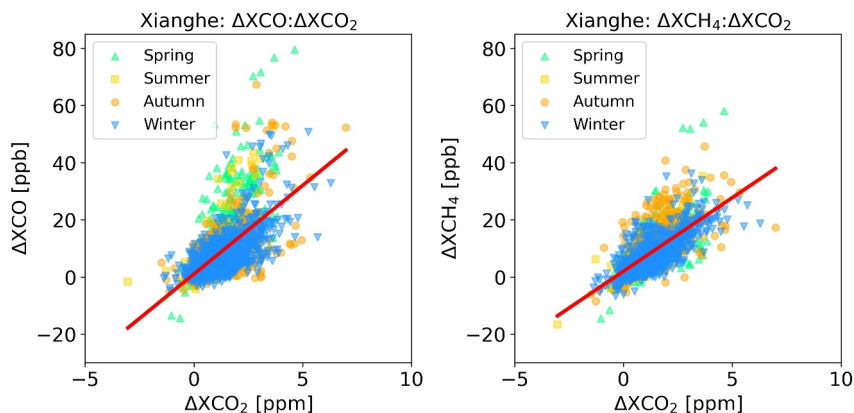
**Figure 3.** Emission ratios (unit: ppb/ppm) of  $\Delta XCO:\Delta XCO_2$  (red bars) and  $\Delta XCH_4:\Delta XCO_2$  (blue bars) for seven urban cities for 2021. The error bars indicate the uncertainties associated with the estimated emission ratios.

Pasadena were attributed not so much to seasonal variations, but rather to the high enhancements of  $XCO_2$ ,  $XCO$ , and  $XCH_4$  in these urban environments. These extensive distributions (i.e., high emissions) in two urban sites were consistent with previous results reported by Yang et al. (2020) for Xianghe and Wunch et al. (2009) for Pasadena.

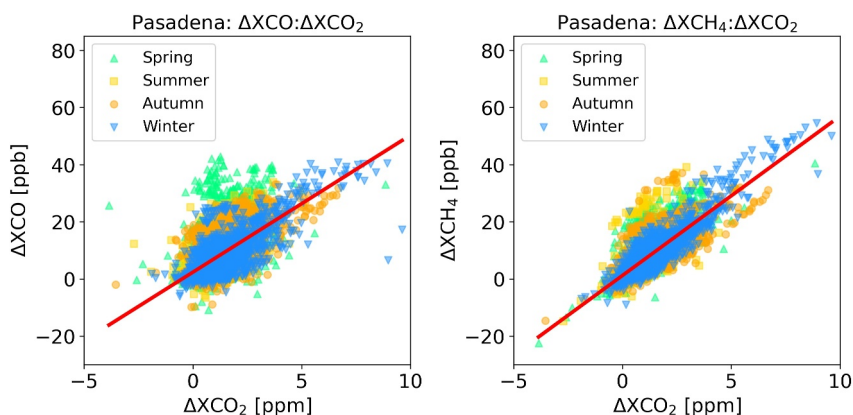
#### 4. Discussion and Conclusions

In this study, we aimed to comprehensively analyze the emission characteristics of GHGs and air pollutants in urban environments and used ground-based FTS measurements for 2021 for this purpose. Our analysis included a comparison of data from seven diverse urban sites in the mid-latitude region of the Northern Hemisphere: Seoul, South Korea; Thessaloniki, Greece; Tsukuba, Japan; Karlsruhe, Germany; Xianghe, China; Pasadena, USA; and Paris, France.

The results showed that Xianghe and Pasadena exhibited the highest  $\Delta XCO:\Delta XCO_2$  emission ratios of  $6.21 \pm 0.15$  ppb/ppm and  $5.94 \pm 0.05$  ppb/ppm, respectively. As mentioned in Section 2.5, the emission ratio was estimated by a slope of the regression lines between two species. Because CO is produced by the incomplete combustion of fossil fuels and shares common combustion sources with  $CO_2$ , the emission ratio of CO and  $CO_2$  serves as an indicator of combustion efficiency or anthropogenic contributions in urban environments (Park, Jeong, Park, et al., 2021; Silva et al., 2013; Wunch et al., 2009). The relatively higher  $\Delta XCO:\Delta XCO_2$  emission ratios in Xianghe and Pasadena suggest lower combustion efficiencies or relatively increased CO emissions, as



**Figure 4.** Scatterplots of (left)  $\Delta XCO$  versus  $\Delta XCO_2$  and (right)  $\Delta XCH_4$  versus  $\Delta XCO_2$  in Xianghe for 2021. Each color in the sub-plots represents a different seasonal data point. The red solid line represents the regression line fitted to the data points.

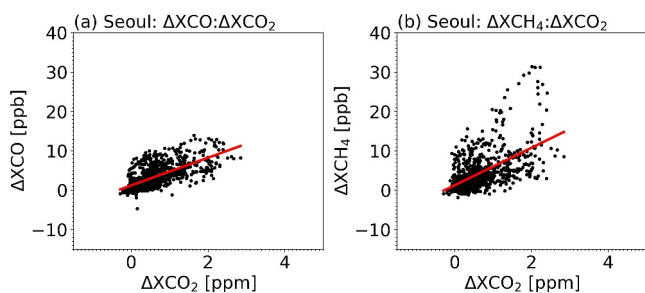


**Figure 5.** Scatterplots of (left)  $\Delta XCO$  versus  $\Delta XCO_2$  and (right)  $\Delta XCH_4$  versus  $\Delta XCO_2$  in Pasadena for 2021. Each color in the sub-plots represents a different seasonal data point. The red solid line represents the regression line fitted to the data points.

observed in the more extensive distributions in Xianghe and Pasadena in Figure 2. Xianghe is located between two megacities in China, Beijing situated approximately 50 km northwest and Tianjin located approximately 70 km southeast (Yang et al., 2020). The city is surrounded by agricultural lands, densely populated areas, and light industries, all of which contribute to the air pollution and degradation of air quality in Xianghe (Li et al., 2007). Pasadena, located at the northern limit of the South Coast Air Basin in the USA, encounters significant air pollution issues owing to its high population density and geographical characteristics, making it one of the most polluted areas in the country (Wunch et al., 2009). Thessaloniki exhibited a ratio of  $5.34 \pm 0.08$  ppb/ppm, which is relatively lower than Xianghe and Pasadena but higher than the other four cities. Thessaloniki is the second-largest city in Greece (Mermigkas et al., 2021) and is known to encounter air pollution issues, primarily attributed to traffic-related emissions (Mermigkas et al., 2021; Vouitsis et al., 2015). Seoul showed a relatively low  $\Delta XCO:\Delta XCO_2$  ratio of  $3.32 \pm 0.10$  ppb/ppm, suggesting lower CO emissions and higher combustion efficiency in the city. The Ministry of Environment of South Korea has implemented several measures and policies to reduce air pollutant emissions in the capital city, as outlined in the second Seoul Metropolitan Air Quality Control Master Plan (2015–2024). These measures include various management strategies related to vehicle emissions, such as the supply of eco-friendly vehicles, reduction of emissions from old cars, and the designation of low-emission zones (Ho et al., 2021). The relatively low  $\Delta XCO:\Delta XCO_2$  ratio in Seoul indicates that these measures and policies effectively reduced air pollution in Seoul. Our findings are further supported by the official bottom-up emission inventory for air pollutants in South Korea, known as the Clean Air Policy Support System (CAPSS) (National Institute of Environmental Research, 2019). According to the CAPSS inventory, CO emissions in Seoul have decreased substantially, by approximately 63%, from 113,309 t in 2011 to 42,125 t in 2020. The relatively low  $\Delta XCO:\Delta XCO_2$  ratio in Seoul is consistent with the results of previous studies (Park, Jeong, Park, et al., 2021; Sim et al., 2020). Based on mobile surveys and building monitoring experiments, Sim et al. (2020) found lower  $\Delta CO:\Delta CO_2$  ratios in Seoul compared to other urban environments, such as Los Angeles.

Park, Jeong, Park, et al. (2021) used satellite observations (OCO-2 and S-5P TROPOMI) to assess the emission characteristics of cities in the Northern Hemisphere and confirmed the relatively low  $\Delta CO:\Delta CO_2$  ratios in Seoul compared to other cities in the Northern Hemisphere. Moreover, the Karlsruhe site, which is a small urban region surrounded by forest (Che et al., 2022), showed the lowest  $\Delta XCO:\Delta XCO_2$  ratio of  $1.91 \pm 0.11$  ppb/ppm among the cities.

In terms of  $\Delta XCH_4:\Delta XCO_2$  ratios, both Pasadena and Xianghe exhibited the highest ratios of  $5.58 \pm 0.04$  ppb/ppm and  $5.15 \pm 0.10$  ppb/ppm, respectively. The  $\Delta XCH_4:\Delta XCO_2$  ratio observed in Pasadena is consistent with those reported in other studies. For instance, Wong et al. (2015) found that the  $\Delta XCH_4:\Delta XCO_2$  ratios in Los Angeles ranged from 5.4 to 7.3 ppb/ppm, which is consistent with our observed value for Pasadena. Xianghe is located



**Figure 6.** Scatterplots of (a)  $\Delta XCO$  versus  $\Delta XCO_2$  and (b)  $\Delta XCH_4$  versus  $\Delta XCO_2$  in Seoul for 2022. The red solid line represents the regression line fitted to the data points.



**Table 2**  
Emission Ratios (Unit: ppb/ppm) of  $\Delta XCO:\Delta XCO_2$  and  $\Delta XCH_4:\Delta XCO_2$  for Xianghe, Paris, Pasadena, and Karlsruhe for 2019–2021

Urban sites	Emission ratios	Year		
		2019	2020	2021
Xianghe (China)	$\Delta XCO:\Delta XCO_2$	$11.41 \pm 0.25$	$7.26 \pm 0.18$	$6.21 \pm 0.15$
	$\Delta XCH_4:\Delta XCO_2$	$5.92 \pm 0.10$	$4.78 \pm 0.08$	$5.15 \pm 0.10$
Pasadena (USA)	$\Delta XCO:\Delta XCO_2$	$4.75 \pm 0.07$	$4.97 \pm 0.05$	$5.94 \pm 0.05$
	$\Delta XCH_4:\Delta XCO_2$	$5.57 \pm 0.04$	$5.83 \pm 0.04$	$5.58 \pm 0.04$
Paris (France)	$\Delta XCO:\Delta XCO_2$	$3.69 \pm 0.06$	$2.52 \pm 0.10$	$2.95 \pm 0.11$
	$\Delta XCH_4:\Delta XCO_2$	$3.37 \pm 0.08$	$2.98 \pm 0.11$	$4.17 \pm 0.12$
Karlsruhe (Germany)	$\Delta XCO:\Delta XCO_2$	$2.12 \pm 0.08$	$2.42 \pm 0.09$	$1.91 \pm 0.11$
	$\Delta XCH_4:\Delta XCO_2$	$3.21 \pm 0.23$	$3.84 \pm 0.13$	$3.99 \pm 0.16$

Note. The results for the year 2021 correspond to those in Figure 3.

in an area with high  $CH_4$  emissions, particularly due to the presence of irrigated croplands in the surrounding region. According to the emissions inventory of the Emission Database for Global Atmosphere Research (Crippa et al., 2018), the estimated  $CH_4$  emissions in Xianghe ranges from 450 to 1,200  $tm^{-2}y^{-1}$  (Ji et al., 2020). Notably, Seoul exhibited a relatively high  $\Delta XCH_4:\Delta XCO_2$  ratio of  $4.85 \pm 0.04$  ppb/ppm, which is comparable to that observed in Xianghe. This suggests significant  $CH_4$  emissions in the city. The sources of  $CH_4$  emissions in urban areas are diverse and include wastewater management, energy production, landfills, and leakage from liquefied natural gas (LNG) infrastructure. These findings are consistent with those reported by Park et al. (2022); they used aircraft emission data to monitor  $CO_2$ ,  $CH_4$ , and CO in Seoul and observed unexpected  $CH_4$  emissions and leakages during the supply of LNG from a large commercial multi-complex building. The presence of such emissions highlights the need for the careful monitoring and control of  $CH_4$  emission sources in Seoul to mitigate these emissions and address climate change.

This study mainly focused on the year 2021 because it was the only year with complete data for all cities. However, to demonstrate the robustness of our analysis, we also examined data from other years, even though the number of comparison urban sites decreased. First, we estimated the emission ratios in Seoul for the year 2022. The EM27/SUN spectrometer in Seoul, South Korea has been operational from May 2020 to the present. Figure 6 shows the scatterplots of  $\Delta XCO$  versus  $\Delta XCO_2$  and  $\Delta XCH_4$  versus  $\Delta XCO_2$  in Seoul for 2022. As mentioned in Section 2.5, the emission ratio is determined by the regression slope between two species. Although there were slight differences of the estimated emission ratios between 2021 and 2022, these differences were not significant. Specifically, the  $\Delta XCO:\Delta XCO_2$  ratio was  $3.52 \pm 0.12$  ppb/ppm, and the  $\Delta XCH_4:\Delta XCO_2$  ratio of  $4.76 \pm 0.21$  ppb/ppm for 2022, compared to  $3.32 \pm 0.10$  ppb/ppm, and  $4.85 \pm 0.04$  ppb/ppm for 2021, respectively. Second, we examined data from 2019 to 2020, for Xianghe, Paris, Pasadena and Karlsruhe—these are the years with complete data for these cities. The estimated emission ratios of  $\Delta XCO:\Delta XCO_2$ ,  $\Delta XCH_4:\Delta XCO_2$  for these years are presented in Table 2. Although the number of urban sites included in the comparisons was fewer and the estimated emission ratios varied, the observed trends remained consistent with the those for the year 2021, our focus year. Specifically, the high emission ratios observed in Xianghe and Pasadena in 2021 were also evident in 2019 and 2020. Similarly, the relatively lower emission ratios in Paris and Karlsruhe demonstrated the consistent patterns across these years. Our analysis from different years suggests that the consistency in emission ratio trends across different years underscores the robustness of our analysis and supports the utility of our approach.

This study has certain limitations. First, the analysis period was limited to 1 year (2021) based on available data. Second, potential spatial variabilities exist in the emissions within the cities, indicating that the estimated emission ratios may not be representative of emissions from all areas of the cities. Despite these limitations, our study demonstrates the effectiveness of ground-based FTS measurements in comprehensively evaluating the emission characteristics in urban environments. Furthermore, the application of our study to longer analysis periods and more sites can support the formulation and implementation of effective strategies for mitigating climate change.

### Conflict of Interest

The authors declare no conflicts of interest relevant to this study.

### Data Availability Statement

The TCCON data sets from Xianghe (Zhou et al., 2022), Pasadena (Wennberg et al., 2022), and Paris (Té et al., 2022) are obtained from the TCCON Data Archive hosted by CaltechData (<https://tccondata.org>). The COCCON data sets from Thessaloniki and Karlsruhe are available at the COCCON Data Repository. They can be accessed directly at the Thessaloniki site (<https://secondary-data-archive.nilu.no/evdc/ftir/coccon/thessaloniki/version1/>) and the Karlsruhe site (<https://secondary-data-archive.nilu.no/evdc/ftir/coccon/karlsruhe/version2/>). The Tsukuba COCCON data sets used in this study for the year 2021 were obtained from the National Institute for Environmental Studies (NIES) in Japan. These data sets can be available by contacting Matthias Max Frey at NIES. Additionally, The Tsukuba COCCON data sets from other years are publicly available at the COCCON Data Repository and can be accessed directly at <https://secondary-data-archive.nilu.no/evdc/ftir/coccon/tsukuba/version2/>. The Seoul COCCON data sets, produced by Seoul National University (SNU) in South Korea, can be available by contacting Hayoung Park at SNU. The OCO-2 data sets are available from NASA Goddard Earth Science Data and Information Service Center (<https://daac.gsfc.nasa.gov/>). The TROPOMI data sets are available from Sentinel-5P Data Hub (<https://dataspace.copernicus.eu/explore-data/data-collections/sentinel-5p/>).

### Acknowledgments

The authors would like to express their gratitude to the editor and anonymous reviewers for providing valuable comments and suggestions that have significantly improved the quality of the paper, and for their time and effort in reviewing our manuscript. The TCCON data were obtained from the TCCON Data Archive hosted by CaltechDATA at <https://tccondata.org>. The COCCON data were obtained from the COCCON Data Repository hosted by KIT at <https://imk-asf.kit.edu/english/3884.php>. We gratefully acknowledge TCCON and COCCON site PIs for the data used in this work. The Paris site has received funding from Sorbonne Université, the French research center CNRS, the French space agency CNES, and Région Île-de-France. The authors acknowledge the efforts of NASA and ESA with respect to providing the OCO-2 and TROPOMI data products. The authors thank Mahesh Kumar Sha for helpful discussions. This work was supported by Korea Environment Industry & Technology Institute (KEITI) through "Climate Change R&D Project for New Climate Regime," funded by Korea Ministry of Environment (MOE) (2022003560006).

### References

- Alberti, C., Hase, F., Frey, M., Dubravica, D., Blumenstock, T., Dehn, A., et al. (2022). Improved calibration procedures for the EM27/SUN spectrometers of the Collaborative Carbon Column Observing Network (COCCON). *Atmospheric Measurement Techniques*, 15(8), 2433–2463. <https://doi.org/10.5194/amt-15-2433-2022>
- Andreae, M. O., & Merlet, P. (2001). Emission of trace gases and aerosols from biomass burning. *Global Biogeochemical Cycles*, 15(4), 955–966. <https://doi.org/10.1029/2000gb001382>
- Bares, R., Lin, J. C., Hoch, S. W., Baasandorj, M., Mendoza, D. L., Fasoli, B., et al. (2018). The wintertime covariation of CO<sub>2</sub> and criteria pollutants in an urban valley of the western United States. *Journal of Geophysical Research-Atmospheres*, 123(5), 2684–2703. <https://doi.org/10.1002/2017jd027917>
- Butz, A., Dinger, A. S., Bobrowski, N., Kostinek, J., Fieber, L., Fischerkeller, C., et al. (2017). Remote sensing of volcanic CO<sub>2</sub>, HF, HCl, SO<sub>2</sub>, and BrO in the downwind plume of Mt. Etna. *Atmospheric Measurement Techniques*, 10(1), 1–14. <https://doi.org/10.5194/amt-10-1-2017>
- Butz, A., Hanft, V., Kleinschek, R., Frey, M. M., Müller, A., Knapp, M., et al. (2022). Versatile and targeted validation of space-borne XCO<sub>2</sub>, XCH<sub>4</sub>, and XCO observations by mobile ground-based direct-sun spectrometers. *Frontiers in Remote Sensing*, 2, 775805. <https://doi.org/10.3389/frsen.2021.775805>
- Chandra, N., Lal, S., Venkataramani, S., Patra, P. K., & Sheel, V. (2016). Temporal variations of atmospheric CO<sub>2</sub> and CO at Ahmedabad in western India. *Atmospheric Chemistry and Physics*, 16(10), 6153–6173. <https://doi.org/10.5194/acp-16-6153-2016>
- Che, K., Liu, Y., Cai, Z. N., Yang, D. X., Wang, H. B., Ji, D. H., et al. (2022). Characterization of regional combustion efficiency using ΔXCO: ΔXCO<sub>2</sub> observed by a portable Fourier-transform spectrometer at an urban site in Beijing. *Advances in Atmospheric Sciences*, 39(8), 1299–1315. <https://doi.org/10.1007/s00376-022-1247-7>
- Crippa, M., Guizzardi, D., Muntean, M., Schaaf, E., Dentener, F., van Aardenne, J. A., et al. (2018). Gridded emissions of air pollutants for the period 1970–2012 within EDGAR v4.3.2. *Earth System Science Data*, 10(4), 1987–2013. <https://doi.org/10.5194/essd-10-1987-2018>
- Crippa, M., Guizzardi, D., Pisoni, E., Solazzo, E., Guion, A., Muntean, M., et al. (2021). Global anthropogenic emissions in urban areas: Patterns, trends, and challenges. *Environmental Research Letters*, 16(7), 074033. <https://doi.org/10.1088/1748-9326/ac00e2>
- Crisp, D., Pollock, H. R., Rosenberg, R., Chapsky, L., Lee, R. A. M., Oyafuso, F. A., et al. (2017). The on-orbit performance of the Orbiting Carbon Observatory-2 (OCO-2) instrument and its radiometrically calibrated products. *Atmospheric Measurement Techniques*, 10(1), 59–81. <https://doi.org/10.5194/amt-10-59-2017>
- Deeter, M. N., Emmons, L. K., Francis, G. L., Edwards, D. P., Gille, J. C., Warner, J. X., et al. (2003). Operational carbon monoxide retrieval algorithm and selected results for the MOPITT instrument. *Journal of Geophysical Research*, 108(D14), 4399. <https://doi.org/10.1029/2002JD003186>
- Eldering, A., O'Dell, C. W., Wennberg, P. O., Crisp, D., Gunson, M. R., Viatte, C., et al. (2017). The Orbiting Carbon Observatory-2: First 18 months of science data products. *Atmospheric Measurement Techniques*, 10(2), 549–563. <https://doi.org/10.5194/amt-10-549-2017>
- Frey, M., Hase, F., Blumenstock, T., Groß, J., Kiel, M., Tsidu, G. M., et al. (2015). Calibration and instrumental line shape characterization of a set of portable FTIR spectrometers for detecting greenhouse gas emissions. *Atmospheric Measurement Techniques*, 8(7), 3047–3057. <https://doi.org/10.5194/amt-8-3047-2015>
- Frey, M., Sha, M. K., Hase, F., Kiel, M., Blumenstock, T., Harig, R., et al. (2019). Building the Collaborative Carbon Column Observing Network (COCCON): Long-term stability and ensemble performance of the EM27/SUN Fourier transform spectrometer. *Atmospheric Measurement Techniques*, 12(3), 1513–1530. <https://doi.org/10.5194/amt-12-1513-2019>
- Gisi, M., Hase, F., Dohe, S., Blumenstock, T., Simon, A., & Keens, A. (2012). XCO<sub>2</sub>-measurements with a tabletop FTS using solar absorption spectroscopy. *Atmospheric Measurement Techniques*, 5(11), 2969–2980. <https://doi.org/10.5194/amt-5-2969-2012>
- Hase, F., Frey, M., Kiel, M., Blumenstock, T., Harig, R., Keens, A., & Orphal, J. (2016). Addition of a channel for XCO observations to a portable FTIR spectrometer for greenhouse gas measurements. *Atmospheric Measurement Techniques*, 9(5), 2303–2313. <https://doi.org/10.5194/amt-9-2303-2016>

- Hedelius, J. K., Liu, J. J., Oda, T., Maksyutov, S., Roehl, C. M., Iraci, L. T., et al. (2018). Southern California megacity CO<sub>2</sub>, CH<sub>4</sub>, and CO flux estimates using ground- and space-based remote sensing and a Lagrangian model. *Atmospheric Chemistry and Physics*, 18(22), 16271–16291. <https://doi.org/10.5194/acp-18-16271-2018>
- Ho, C. H., Heo, J. W., Chang, M., Choi, W., Kim, J., Kim, S. W., & Oh, H. R. (2021). Regulatory measures significantly reduced air-pollutant concentrations in Seoul, Korea. *Atmospheric Pollution Research*, 12(7), 101098. <https://doi.org/10.1016/j.apr.2021.101098>
- IPCC. (2007). In S. Solomon, D. Qin, M. Manning, Z. Chen, M. Marquis, K. B. Averyt, et al. (Eds.), *Climate Change 2007: The Physical Science Basis. Contribution of Working Group I to the Fourth Assessment Report of the International Panel on Climate Change* (p. 996). Cambridge University Press.
- Ji, D. H., Zhou, M. Q., Wang, P. C., Yang, Y., Wang, T., Sun, X. Y., et al. (2020). Deriving temporal and vertical distributions of methane in Xianghe using ground-based Fourier transform infrared and gas-analyzer measurements. *Advances in Atmospheric Sciences*, 37(6), 597–607. <https://doi.org/10.1007/s00376-020-9233-4>
- Klappenbach, F., Bertleff, M., Kostinek, J., Hase, F., Blumenstock, T., Agusti-Panareda, A., et al. (2015). Accurate mobile remote sensing of XCO<sub>2</sub> and XCH<sub>4</sub> latitudinal transects from aboard a research vessel. *Atmospheric Measurement Techniques*, 8(12), 5023–5038. <https://doi.org/10.5194/amt-8-5023-2015>
- Knapp, M., Kleinschek, R., Hase, F., Agusti-Panareda, A., Inness, A., Barre, J., et al. (2021). Shipborne measurements of XCO<sub>2</sub>, XCH<sub>4</sub>, and XCO above the Pacific Ocean and comparison to CAMS atmospheric analyses and S5P/TROPOMI. *Earth System Science Data*, 13(1), 199–211. <https://doi.org/10.5194/essd-13-199-2021>
- Kuze, A., Suto, H., Nakajima, M., & Hamazaki, T. (2009). Thermal and near infrared sensor for carbon observation Fourier-transform spectrometer on the Greenhouse Gases Observing Satellite for greenhouse gases monitoring. *Applied Optics*, 48(35), 6716–6733. <https://doi.org/10.1364/AO.48.006716>
- Laughner, J. L., Roche, S., Kiel, M., Toon, G. C., Wunch, D., Baier, B. C., et al. (2023). A new algorithm to generate a priori trace gas profiles for the GGG2020 retrieval algorithm. *Atmospheric Measurement Techniques*, 16(5), 1121–1146. <https://doi.org/10.5194/amt-16-1121-2023>
- Li, C., Marufu, L. T., Dickerson, R. R., Li, Z. Q., Wen, T. X., Wang, Y. S., et al. (2007). In situ measurements of trace gases and aerosol optical properties at a rural site in northern China during East Asian Study of Tropospheric Aerosols: An International Regional Experiment 2005. *Journal of Geophysical Research*, 112(D22), D22S04. <https://doi.org/10.1029/2006jd007592>
- Luther, A., Kleinschek, R., Scheidweiler, L., Defratyka, S., Stanisavljevic, M., Forstmaier, A., et al. (2019). Quantifying CH<sub>4</sub> emissions from hard coal mines using mobile sun-viewing Fourier transform spectrometry. *Atmospheric Measurement Techniques*, 12(10), 5217–5230. <https://doi.org/10.5194/amt-12-5217-2019>
- Makarova, M. V., Alberti, C., Ionov, D. V., Hase, F., Foka, S. C., Blumenstock, T., et al. (2021). Emission Monitoring Mobile Experiment (EMME): An overview and first results of the St. Petersburg megacity campaign 2019. *Atmospheric Measurement Techniques*, 14(2), 1047–1073. <https://doi.org/10.5194/amt-14-1047-2021>
- Mermigkas, M., Topaloglou, C., Balis, D., Koukoulis, M. E., Hase, F., Dubravica, D., et al. (2021). FTIR measurements of greenhouse gases over Thessaloniki, Greece in the framework of COCCON and comparison with S5P/TROPOMI observations. *Remote Sensing*, 13(17), 3395. <https://doi.org/10.3390/rs13173395>
- National Institute of Environmental Research. (2019). 2016 National Air Pollutants Emissions.
- O'Dell, C. W., Connor, B., Bosch, H., O'Brien, D., Frankenberg, C., Castano, R., et al. (2012). The ACOS CO<sub>2</sub> retrieval algorithm – Part 1: Description and validation against synthetic observations. *Atmospheric Measurement Techniques*, 5(1), 99–121. <https://doi.org/10.5194/amt-5-99-2012>
- Pak, N. M., Hedelius, J. K., Roche, S., Cunningham, L., Baier, B., Sweeney, C., et al. (2023). Using portable low-resolution spectrometers to evaluate Total Carbon Column Observing Network (TCCON) biases in North America. *Atmospheric Measurement Techniques*, 16(5), 1239–1261. <https://doi.org/10.5194/amt-16-1239-2023>
- Park, H., Jeong, S., Koo, J. H., Sim, S., Bae, Y., Kim, Y., et al. (2021). Lessons from COVID-19 and Seoul: Effects of reduced human activity from social distancing on urban CO<sub>2</sub> concentration and air quality. *Aerosol and Air Quality Research*, 21(1), 200376. <https://doi.org/10.4209/aaqr.2020.07.0376>
- Park, H., Jeong, S., Park, H., Kim, Y., Park, C., Sim, S., et al. (2022). Unexpected urban methane hotspots captured from aircraft observations. *ACS Earth and Space Chemistry*, 6(3), 755–765. <https://doi.org/10.1021/acsearthspacechem.1c00431>
- Park, H., Jeong, S., Park, H., Labzovskii, L. D., & Bowman, K. W. (2021). An assessment of emission characteristics of Northern Hemisphere cities using spaceborne observations of CO<sub>2</sub>, CO, and NO<sub>2</sub>. *Remote Sensing of Environment*, 254, 112246. <https://doi.org/10.1016/j.rse.2020.112246>
- Sha, M. K., De Mazière, M., Notholt, J., Blumenstock, T., Chen, H., Dehn, A., et al. (2020). Intercomparison of low- and high-resolution infrared spectrometers for ground-based solar remote sensing measurements of total column concentrations of CO<sub>2</sub>, CH<sub>4</sub>, and CO. *Atmospheric Measurement Techniques*, 13(9), 4791–4839. <https://doi.org/10.5194/amt-13-4791-2020>
- Sha, M. K., Langerock, B., Blavier, J. F. L., Blumenstock, T., Borsdorff, T., Buschmann, M., et al. (2021). Validation of methane and carbon monoxide from Sentinel-5 Precursor using TCCON and NDACC-IRWG stations. *Atmospheric Measurement Techniques*, 14(9), 6249–6304. <https://doi.org/10.5194/amt-14-6249-2021>
- Silva, S. J., Arellano, A. F., & Worden, H. M. (2013). Toward anthropogenic combustion emission constraints from space-based analysis of urban CO<sub>2</sub>/CO sensitivity. *Geophysical Research Letters*, 40(18), 4971–4976. <https://doi.org/10.1002/grl.50954>
- Sim, S., Jeong, S., Park, H., Park, C., Kwak, K.-H., Lee, S.-B., et al. (2020). Co-benefit potential of urban CO<sub>2</sub> and air quality monitoring: A study on the first mobile campaign and building monitoring experiments in Seoul during the winter. *Atmospheric Pollution Research*, 11(11), 1963–1970. <https://doi.org/10.1016/j.apr.2020.08.009>
- Té, Y., Jeseck, P., & Janssen, C. (2022). *TCCON data from Paris, France, Release GGG2020R0. TCCON data archive, hosted by CaltechDATA*. California Institute of Technology. <https://doi.org/10.14291/tcon.ggg2020.paris01.R0>
- Veefkind, J. P., Aben, I., McMullan, K., Forster, H., de Vries, J., Otter, G., et al. (2012). TROPOMI on the ESA Sentinel-5 Precursor: A GMES mission for global observations of the atmospheric composition for climate, air quality and ozone layer applications. *Remote Sensing of Environment*, 120, 70–83. <https://doi.org/10.1016/j.rse.2011.09.027>
- Viatte, C., Lauvaux, T., Hedelius, J. K., Parker, H., Chen, J., Jones, T., et al. (2017). Methane emissions from dairies in the Los Angeles Basin. *Atmospheric Chemistry and Physics*, 17(12), 7509–7528. <https://doi.org/10.5194/acp-17-7509-2017>
- Vouitsis, I., Amanatidis, S., Ntziachristos, L., Kelessis, A., Petrakakis, M., Stamos, I., et al. (2015). Daily and seasonal variation of traffic related aerosol pollution in Thessaloniki, Greece, during the financial crisis. *Atmospheric Environment*, 122, 577–587. <https://doi.org/10.1016/j.atmosenv.2015.10.008>
- Wennberg, P. O., Mui, W., Wunch, D., Kort, E. A., Blake, D. R., Atlas, E. L., et al. (2012). On the sources of methane to the Los Angeles atmosphere. *Environmental Science & Technology*, 46(17), 9282–9289. <https://doi.org/10.1021/es301138y>

- Wennberg, P. O., Wunch, D., Roehl, C., Blavier, J.-F., Toon, G. C., & Allen, N. (2022). *TCCON data from California Institute of Technology, Pasadena, California, USA, Release GGG2020R0*. *TCCON data archive, hosted by CaltechDATA*. California Institute of Technology. <https://doi.org/10.14291/tcon.ggg2020.pasadena01.R0>
- Wong, K. W., Fu, D., Pongetti, T. J., Newman, S., Kort, E. A., Duren, R., et al. (2015). Mapping CH<sub>4</sub>:CO<sub>2</sub> ratios in Los Angeles with CLARS-FTS from Mount Wilson, California. *Atmospheric Chemistry and Physics*, *15*(1), 241–252. <https://doi.org/10.5194/acp-15-241-2015>
- Worthy, D. E. J., Chan, E., Ishizawa, M., Chan, D., Poss, C., Dlugokencky, E. J., et al. (2009). Decreasing anthropogenic methane emissions in Europe and Siberia inferred from continuous carbon dioxide and methane observations at Alert, Canada. *Journal of Geophysical Research*, *114*(D10), D10301. <https://doi.org/10.1029/2008JD011239>
- Wunch, D., Toon, G. C., Blavier, J. F. L., Washenfelder, R. A., Notholt, J., Connor, B. J., et al. (2011). The total carbon column observing network. *Philosophical Transactions of the Royal Society A: Mathematical, Physical & Engineering Sciences*, *369*(1943), 2087–2112. <https://doi.org/10.1098/rsta.2010.0240>
- Wunch, D., Toon, G. C., Sherlock, V., Deutscher, N. M., Liu, C., Feist, D. G., & Wennberg, P. O. (2015). *Documentation for the 2014 TCCON Data Release (GGG2014.R0)*. CaltechDATA. <https://doi.org/10.14291/TCCON.GGG2014.DOCUMENTATION.R0/1221662>
- Wunch, D., Wennberg, P. O., Toon, G. C., Keppel-Aleks, G., & Yavin, Y. G. (2009). Emissions of greenhouse gases from a North American megacity. *Geophysical Research Letters*, *36*(15), L15810. <https://doi.org/10.1029/2009GL039825>
- Yang, Y., Zhou, M. Q., Langerock, B., Sha, M. K., Hermans, C., Wang, T., et al. (2020). New ground-based Fourier-transform near-infrared solar absorption measurements of XCO<sub>2</sub>, XCH<sub>4</sub> and XCO at Xianghe, China. *Earth System Science Data*, *12*(3), 1679–1696. <https://doi.org/10.5194/essd-12-1679-2020>
- Zhou, M., Wang, P., Nan, W., Yang, Y., Kumps, N., Hermans, C., & De Mazière, M. (2022). *TCCON data from Xianghe, China, Release GGG2020R0*. *TCCON data archive, hosted by CaltechDATA*. California Institute of Technology. <https://doi.org/10.14291/tcon.ggg2020.xianghe01.R0>